Key Engineering Materials
ISSN: 1662-9795, Vol. 926, pp 305-315
doi:10.4028/p-r0d8ov

Submitted: 2021-12-07
Accepted: 2022-02-18
Online: 2022-07-22

Prediction of Solid-State Phase Transformations for the Ti-6Al-4V Alloy

Carlos M. Andrade[1,a*], Diogo M. Neto[1,b] and Marta C. Oliveira[1,c]

[1]CEMMPRE, Department of Mechanical Engineering, University of Coimbra, Pinhal de Marrocos, 3030-788 Coimbra, Portugal

[a]carlos.andrade@uc.pt, [b]diogo.neto@dem.uc.pt, [c]marta.oliveira@dem.uc.pt

Keywords: Selective Laser Melting; Microstructure; Phase transformations; Phase volume fraction

Abstract. Ti-6Al-4V alloy is the most relevant titanium alloy, finding applications in multiple high-value industries. The production of Ti-6Al-4V components by selective laser melting is particularly challenging, due to the highly localized heat input and large temperature gradients, which affect the material's microstructure and final mechanical properties. The main objective of this work is to develop a metallurgical framework able to describe the solid-state phase transformations of Ti-6Al-4V during processing. The predicted volume fraction of each solid phase is used to estimate strains induced by the thermal cycle and the phase transformations independently. The presented numerical model considers a single finite element subjected to heat fluxes that impose two sequential heating/cooling cycles, replicating the laser movement. The numerical results emphasize the importance of predicting phase volume fraction fields for an accurate estimation of the material's volume change. In fact, changing the heating/cooling rates resulted in completely different final microstructures and a 0.5% difference on the material's volume change relative to its initial volume, which would correspond to a stress increment of approximately 200 MPa if the linear elastic material was fully constrained.

Introduction

Currently, Selective Laser Melting (SLM) is one of the main additive manufacturing processes for the production of metallic components. This process is highly complex and governed by multiple competing physical effects, requiring the fine-tuning of numerous process parameters to avoid part defects or even failure. Among the metallic materials processed by SLM, the Ti-6Al-4V alloy is one of the most relevant in the market, finding applications in multiple high-value industries [1]. The evolution of the microstructure of Ti-6Al-4V parts can be particularly complex, since the SLM process is associated with an extremely localized heat input and high temperature gradients [2]. According to the thermal history, the microstructure can contain α, β and α' martensite. Although not very commonly, small volume fractions of α″ martensite can also be found in regions enriched with β-stabilizing elements (such as vanadium, V) [3]. Typically, at room temperature, as-built parts consist predominantly of α' martensite, since the high cooling rates promote the martensitic transformation from the β phase [4]. Nevertheless, under a combination of specific process parameters, the in-process temperatures and the time at high temperatures during the thermal cycles can be increased, promoting the decomposition of α' into α and β phases [5][6].

Since the complex thermal cycles imposed on the material are directly related to the resulting microstructure, numerical simulations of the SLM process should include the microstructure prediction. This is achieved by incorporating a metallurgical framework in the classical thermo-mechanical model. Following this approach, it is possible to determine the final part properties from the meso-scale analysis of the SLM process, ensuring fundamental understanding of the process-structure-property-performance link, which provides the basis for the process optimization [7]. One of the most common options to describe the evolution of the solid phases of a material is by adopting phenomenological models. Tan et al. [8] developed a multi-track multi-layer thermo-metallurgical-mechanical model for SLM simulation of Ti-6Al-4V builds. The numerical results showed that the consideration of solid-state phase transformations led to the decrease of tensile residual stresses and

the increase of compressive residual stresses. Fan et al. [9] developed a thermo-metallurgical-mechanical model to study the laser forming of Ti-6Al-4V, considering the effect of solid-state phase transformations on the material's flow behavior. Moreover, several plates were laser scanned and their bending angles were experimentally measured. The numerically predicted phase volume fractions and bending angles were shown to be in good agreement with the experimental results.

In this work, a metallurgical framework to predict the microstructure evolution of the Ti-6Al-4V alloy is integrated in a thermo-mechanical finite element model. Three solid phases are considered: α, β and α'. The martensitic transformation is modelled using an adapted Koistinen-Marburger equation [10], valid for arbitrary thermal histories. The diffusional transformations are modelled using a modified Johnson-Mehl-Avrami equation [11], able to describe non-isothermal conditions. The thermal problem is solved and its solution is used as input to the equations that describe the phase transformations, which provide the evolution of the volume fraction of each phase. In turn, these values influence the mechanical model *via* the thermal strain and the volume change strain associated to each transformation. To better isolate the effect of the solid phase transformations, all material properties are assumed temperature independent with exception of the thermal expansion coefficients. The numerical model considers a single finite element subjected to heat fluxes that impose the desired temperature evolution, replicating the laser motion.

Microstructure of Ti-6Al-4V Alloy

At room temperature, the microstructure of Ti-6Al-4V is composed of hexagonal close-packed (hcp) α and body-centered cubic (bcc) β phases. Despite being a high temperature phase, the β phase is present at room temperature due to the effect of vanadium, which acts as a β-stabilizer element.

If the material is heated up to liquid state and then cooled, it will solidify entirely to β phase. Between the melting point and the so-called β-transus temperature only β phase exists. Slow cooling below this temperature promotes the β → α transformation through a diffusional mechanism. If the cooling rate is high enough, the β phase undergoes a non-diffusional transformation, originating a supersaturated hexagonal α' martensite [12]. However, the transformation only starts when the temperature is lower than the martensite start temperature. Since this temperature is affected by the alloying elements, different values have been reported in the literature, ranging from 575 °C to 800 °C [5]. Cooling rates above 410 °C/s originate a fully martensitic microstructure; cooling rates between 410 and 20 °C/s lead to incomplete transformation to α′ and for cooling rates lower than 20 °C/s no α′ is formed [13].

Heating a microstructure consisting of α + β promotes the α → β diffusional transformation. If the material is quenched from the α + β region and there is a high enough concentration of β-stabilizers in the β phase, a second type of martensite can be formed, known as α'' [14]. This martensite is a supersaturated orthorhombic phase, rarely observed in Ti-6Al-4V, due to the low vanadium content. If heated, both α' and α'' decompose into α and β phases, through a diffusional transformation [12].

Thermo-Metallurgical-Mechanical Modelling

In the present study, the metallurgical framework to evaluate the solid-state phase transformations in the Ti-6Al-4V alloy is integrated in a 3D thermo-mechanical model. This approach enables the evaluation of the transient temperature field, the volume fraction of each solid phase and the resulting stress distribution that fulfill the mechanical equilibrium.

Thermal model. The differential equation that governs the transient heat conduction within a continuous medium with arbitrary volume can be derived from the first law of thermodynamics. Assuming that there is no volumetric heat generation, this equation can be expressed as:

$$k\left(\frac{\partial^2 T}{\partial x^2}+\frac{\partial^2 T}{\partial y^2}+\frac{\partial^2 T}{\partial z^2}\right)=\rho c_{\mathrm{p}}\frac{\partial T}{\partial t}, \tag{1}$$

where k is the thermal conductivity coefficient, ρ denotes the mass density and c_p is the specific heat. The solution of this equation provides the distribution of the transient spatial temperature $T(x,y,z,t)$.

Metallurgical framework. The metallurgical model considers three solid phases: α, β and α'. According to the temperature and heating/cooling rate conditions, four transformations can occur between the phases: a martensitic transformation and three diffusional transformations.

The martensitic transformation, β → α', is modelled using the equation of Koistinen-Marburger [10]. Under arbitrary thermal histories and using a backward Euler integration, the evolution of the volume fraction (f) of martensite can be expressed as [15]:

$$f_{\alpha'}(T+\Delta T)=\frac{f_{\alpha'}(T)-\gamma\Delta T\left(f_{\beta}(T_0)-f_{\beta_r}+f_{\alpha'}(T_0)\right)}{1-\gamma\Delta T}, \tag{2}$$

where γ is the transformation coefficient (which is assigned the value of 0.015 ºC^{-1}), T_0 is the temperature at the beginning of the current cooling cycle and f_{β_r} is the volume fraction of the retained β phase. The latter can be determined based on the initial amount of β using the following relation:

$$f_{\beta_r}=\begin{cases} f_{\beta}(T_0) & ,f_{\beta}(T_0)<0.25 \\ 0.25\,(1-f_{\beta}(T_0)) & ,f_{\beta}(T_0)\geq 0.25 \end{cases}. \tag{3}$$

It is assumed that the martensitic transformation only occurs if the cooling rate is greater than or equal to 410 ºC/s. Moreover, the martensitic start temperature is set to 650 ºC [16].

All the diffusional transformations are modelled using an adapted version of the original Johnson-Mehl-Avrami equation [11], able to describe non-isothermal conditions. This is achieved by using the additivity rule, where continuous cooling is replaced by a series of small consecutive isothermal steps [17]. Thus, the decomposition of α' (α' → α + β) can be expressed as [15]:

$$f_{\alpha'}\left(T+\Delta T\right)=1-\left[1-\exp\left(-k_1\left(\zeta_{\alpha'}+\Delta t\right)^{n_1}\right)\right]\left(1-f_{\alpha'}^{\mathrm{eq}}\right), \text{ if } f_{\alpha'}>f_{\alpha'}^{\mathrm{eq}}, \tag{4}$$

where k_1 is the reaction rate constant, n_1 is the Avrami exponent, Δt is the time step size, $f_{\alpha'}^{\mathrm{eq}}$ is the equilibrium volume fraction of martensite and $\zeta_{\alpha'}$ is the fictitious time which would provide the same amount of transformation that results in volume fraction $f_{\alpha'}(T)$, at a constant temperature $T+\Delta T$, defined as:

$$\zeta_{\alpha'}=\left[-\frac{1}{k_1}\ln\left(\frac{f_{\alpha'}(T)-f_{\alpha'}^{\mathrm{eq}}}{1-f_{\alpha'}^{\mathrm{eq}}}\right)\right]^{\frac{1}{n_1}}. \tag{5}$$

The values of the parameters k_1 and n_1 adopted in this work were determined by Mur et al. [18]. Heating up the martensite leads to its decomposition into equilibrium proportions of α and β, i.e.:

$$\Delta f_{\alpha}\left(T+\Delta T\right)=-\Delta f_{\alpha'}\left(T+\Delta T\right)f_{\alpha,0}^{\mathrm{eq}}\left(T+\Delta T\right), \tag{6}$$

$$\Delta f_{\beta}\left(T+\Delta T\right)=-\Delta f_{\alpha'}\left(T+\Delta T\right)f_{\beta,0}^{\mathrm{eq}}\left(T+\Delta T\right), \tag{7}$$

where $f_{\alpha,0}^{\mathrm{eq}}$ and $f_{\beta,0}^{\mathrm{eq}}$ are the equilibrium volume fractions of α and β in a microstructure containing only these two phases. These volume fractions are determined using the following equations [19]:

$$f_{\alpha,0}^{\mathrm{eq}}(T)=\begin{cases} c_3\left(1-\exp(-c_4(T_{\beta\text{-transus}}-T))\right) & ,T\leq T_{\beta\text{-transus}} \\ 0 & ,T>T_{\beta\text{-transus}} \end{cases}, \tag{8}$$

$$f_{\beta,0}^{eq}(T) = 1 - f_{\alpha,0}^{eq}(T), \tag{9}$$

where the constants assume the values $c_3 = 0.925$, $c_4 = 0.0085$ ºC^{-1} and $T_{\beta\text{-transus}}$ is 980 ºC.

If the microstructure contains α', the equilibrium volume fraction of β depends on the volume fraction of α' as follows:

$$f_{\beta}^{eq}(T) = f_{\beta,0}^{eq}(T)(1 - f_{\alpha'}). \tag{10}$$

The equilibrium volume fraction of α' is approximated by [20]:

$$f_{\alpha'}^{eq}(T) = \frac{1}{2}\left(1 + \tanh\left(\frac{c_1 - T}{c_2}\right)\right), \tag{11}$$

where the constants assume the values $c_1 = 450$ ºC and $c_2 = 80$ ºC.

The α → β and β → α transformations are described, respectively, by [15]:

$$f_{\beta}(T + \Delta T) = \left[1 - \exp\left(-k_2\left(\zeta_{\beta}^{\,h} + \Delta t\right)^{n_2}\right)\right] f_{\beta}^{eq}, \text{ if } f_{\beta} < f_{\beta}^{eq}(T + \Delta T), \tag{12}$$

$$f_{\beta}(T + \Delta T) = 1 - f_{\alpha'} - \left[1 - \exp\left(-k_2\left(\zeta_{\beta}^{\,c} + \Delta t\right)^{n_2}\right)\right]\left(1 - f_{\alpha'} - f_{\beta}^{eq}\right), \text{ if } f_{\beta} > f_{\beta}^{eq}(T + \Delta T), \tag{13}$$

where $\zeta_{\beta}^{\,h}$ (heating) and $\zeta_{\beta}^{\,c}$ (cooling) are given, respectively, by:

$$\zeta_{\beta}^{\,h} = \left[-\frac{1}{k_2}\ln\left(\frac{f_{\beta}^{eq} - f_{\beta}(T)}{f_{\beta}^{eq}}\right)\right]^{\frac{1}{n_2}}, \tag{14}$$

$$\zeta_{\beta}^{\,c} = \left[-\frac{1}{k_2}\ln\left(\frac{f_{\beta}(T) - f_{\beta}^{eq}}{1 - f_{\alpha'} - f_{\beta}^{eq}}\right)\right]^{\frac{1}{n_2}}. \tag{15}$$

The parameters k_2 and n_2 adopted in this work were determined by Malinov et al. [21].

In the proposed metallurgical framework, the cooling rate dictates either β → α or β → α' during a cooling cycle. During heating, both α → β and α' → α + β can occur.

Mechanical model. In order to obtain the mechanical response of the material, the quasi-static mechanical analysis is carried out using the current temperature field (obtained from the thermal analysis) and the volume fractions of the solid phases (given by the metallurgical model). The balance of linear momentum in any point of a solid body is given by:

$$\mathrm{div}(\boldsymbol{\sigma}) + \mathbf{b} = \mathbf{0}, \tag{16}$$

where $\boldsymbol{\sigma}$ is the stress tensor and $\mathbf{b}$ are the body forces, which are neglected in the present model. The total strain increment is given by the sum of the following terms:

$$\boldsymbol{\varepsilon}^{\text{total}} = \boldsymbol{\varepsilon}^{\text{e}} + \boldsymbol{\varepsilon}^{\text{p}} + \boldsymbol{\varepsilon}^{\text{th}} + \boldsymbol{\varepsilon}^{\text{sspt}}, \tag{17}$$

where $\boldsymbol{\varepsilon}^{\text{e}}$ is the elastic strain increment, $\boldsymbol{\varepsilon}^{\text{p}}$ is the plastic strain increment, $\boldsymbol{\varepsilon}^{\text{th}}$ is the thermal strain increment and $\boldsymbol{\varepsilon}^{\text{sspt}}$ is the strain induced by solid-state phase transformations.

The elastic constitutive law defines a linear relationship between the stress tensor and the strain tensor. Thus, the resulting stress from the elastic strain is expressed as:

$$\boldsymbol{\sigma} = \mathbf{C}^{\mathrm{e}} : \boldsymbol{\varepsilon}^{\mathrm{e}}, \tag{18}$$

where $\mathbf{C}^{\mathrm{e}}$ is the fourth-order material stiffness tensor (Elastic moduli). Assuming a linear isotropic elastic material, the stiffness matrix $\mathbf{C}^{\mathrm{e}}$ can be calculated from the Young's modulus (E) and the Poisson's ratio (v).

Considering an associated flow rule in the plasticity model, the plastic strain increment is given by:

$$\Delta\boldsymbol{\varepsilon}^{\mathrm{p}} = \Delta\lambda \frac{\partial F(\boldsymbol{\sigma})}{\partial \boldsymbol{\sigma}}, \tag{19}$$

where $\Delta\lambda$ is the plastic multiplier increment, calculated through the consistency condition, and $F(\boldsymbol{\sigma})$ is the yield criterion. The plastic behavior is also assumed as isotropic and described by the von Mises yield criterion and a perfectly plastic law.

The material expansion/contraction due to heating/cooling is accounted in the thermal strain increment. Nevertheless, since the material can undergo solid-state phase transformations, their effect must be removed from the thermal strain increment, yielding:

$$\Delta\boldsymbol{\varepsilon}^{\mathrm{th}} = \begin{cases} \left[\alpha_{\beta} f_{\beta} + \alpha_{\alpha}\left(1 - f_{\beta}\right)\right]\Delta T\,\mathbf{I} & \text{No transformation} \\ \left[\alpha_{\beta} f_{\beta} + \alpha_{\alpha}\left(1 - f_{\beta} - \Delta f_{\alpha'}\right)\right]\Delta T\,\mathbf{I} & \beta \rightarrow \alpha' \\ \left[\alpha_{\beta} f_{\beta} + \alpha_{\alpha}\left(1 - f_{\beta} - \Delta f_{\alpha}\right)\right]\Delta T\,\mathbf{I} & \beta \rightarrow \alpha \\ \left[\alpha_{\beta}\left(f_{\beta} - \Delta f_{\beta}\right) + \alpha_{\alpha}\left(1 - f_{\beta} - \Delta f_{\alpha,\mathrm{m}}\right)\right]\Delta T\,\mathbf{I} & \alpha \rightarrow \beta \text{ or } \alpha' \rightarrow \alpha + \beta \end{cases}, \tag{20}$$

where α_{α} and α_{β} are the linear thermal expansion coefficients of the α and β phases, respectively, $\Delta f_{\alpha,\mathrm{m}}$ is the increment of volume fraction of α phase from the martensite decomposition transformation and **I** denotes the second-order identity tensor. In this study, we consider that α and α' have the same value of linear thermal expansion coefficient. This assumption is valid since the lattice parameters of the α and α' phases are similar [22]. The last branch of Eq. (20) allows the calculation of the thermal strain if either one of the α → β or α' → α + β transformations occur or if they occur sequentially.

The incremental strain induced by a solid-state phase transformation is given by:

$$\Delta\boldsymbol{\varepsilon}^{\mathrm{sspt}} = \boldsymbol{\varepsilon}^{\Delta \mathrm{V}}(T)\Delta f_i(T), \tag{21}$$

where $\boldsymbol{\varepsilon}^{\Delta \mathrm{V}}$ is the strain induced by the volumetric change associated with a full solid-state phase transformation and $f_{\mathrm{i}}(T)$ is the phase volume fraction occurring in a time increment. The former can be determined from the unit cell volumes of the crystal structures of the phases involved in the solid-state phase transformation. For the α → β transformation:

$$\boldsymbol{\varepsilon}^{\Delta \mathrm{V}} = \frac{\sqrt[3]{V_{\beta}} - \sqrt[3]{V_{\alpha}}}{\sqrt[3]{V_{\alpha}}}, \tag{22}$$

where V_{α} and V_{β} are unit cell volumes of α and β phases, respectively. Due to the similarities in lattice parameters, the values of V_{α} are adopted for the unit cell volume of the α' phase. In this work, the model considers the temperature-dependent values of V_{α} and V_{β} determined by Elmer et al. [23].

Finite element Model

The numerical simulations were carried out with the in-house finite element code DD3IMP, originally developed to simulate sheet metal forming processes [24]. The solution of the transient heat conduction problem is obtained by time integration using the Euler's backward method [25]. The evolution of the deformation is described by an updated Lagrangian scheme. In each increment, an explicit approach is used to calculate a trial solution for the deformation, which is iteratively corrected using a fully implicit Newton–Raphson scheme. The same finite element mesh is adopted in the thermal, metallurgical and mechanical problems (consisting of only 8-node hexahedral elements). However, full integration is adopted in the thermal problem, while the mechanical problem uses the selective reduced integration technique [26] to avoid volumetric locking.

Problem conditions. The proposed numerical model comprises a simple cube with 50 mm of side length, which is modelled with a single finite element in order to obtain uniform temperature and phase volume fraction fields in the whole domain. The cube is initially in powder state and is subjected to two sequential heating/cooling cycles *via* the imposition of heat fluxes in two opposite faces, as illustrated in Fig. 1 (a).

Four numerical simulations were carried out, considering the initial temperature of the material as 25 ºC. The values of the heat fluxes (Q_1 to Q_4) and the corresponding time for their application (t_1 to t_4) are listed in Table 1. Under these conditions, the temperature profile presented in Fig. 1 (b) is obtained, with two sequential heating/cooling cycles. The effect of the solid-state phase transformations on the numerical solution is neglected in simulations 3 and 4, assuming either the thermal expansion coefficient of the α or β phase, respectively. Thus, the volume change in the simulations is different. Therefore, the areas of the faces where the heat fluxes are imposed are slightly different at the beginning of each cooling and reheating cycle, requiring small changes in the prescribed heat flux to obtain the same temperature evolution.

Table 1 – Heat flux [W/mm^2] and time [s] associated to each heating and cooling cycle.

	Q_1	Q_2	Q_3	Q_4	t_1	t_2	t_3	t_4
Simulation 1	57.7	100.54	0.1891	11.82	1	2	252	256
Simulation 2	57.7	6.657	1.8715	47.10	1	16	41	42
Simulation 3	57.7	101	0.1895	11.85	1	2	252	256
Simulation 4	57.7	99.9	0.1862	11.65	1	2	252	256

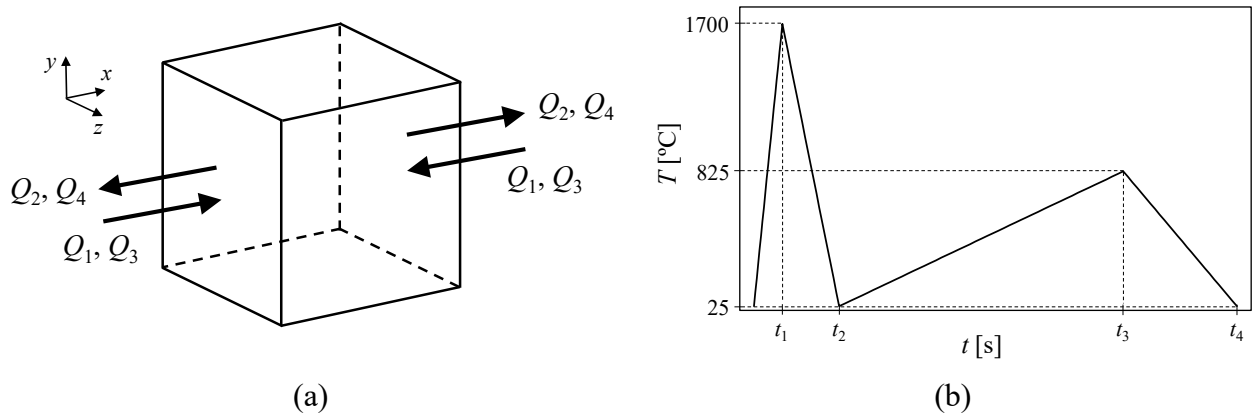

(a) (b)

Fig. 1 – Numerical model: (a) Imposed boundary conditions; (b) Obtained temperature profile.

Material properties. Three material phases (powder, liquid and solid) were considered in the simulations. The powder material switches to liquid when the temperature rises to the melting point (1650 ºC) and the liquid solidifies when the temperature cools below the melting point. Since the main focus of the study is to predict the volume fractions of the solid phases and its influence on the volume change strain (in combination with the thermal strain), all solid material properties were

considered temperature-independent, except the thermal expansion coefficient. The material properties considered temperature independent in the numerical simulations are listed in Table 2. The physical and mechanical properties adopted in the simulations for the solid and liquid Ti-6Al-4V were taken from [27] and [28], respectively. The physical properties of the powder were taken from [29]. Regarding the mechanical strength of the powder and liquid phases, they are considered very weak, using values of Young modulus and yield strength (σ_Y) about 0.1% of the corresponding solid material's values. Note that the mass density of the powder phase is 60% of the solid phase, due to the assumption of 0.6 for the packing factor of the powder bed [30].

Fig. 2 presents the temperature dependent thermal expansion coefficients for the α and β solid phases (calculated from the lattice parameters experimentally determined by Elmer et al. [23]). The thermal expansion of the powder and liquid phases is neglected in the present study. Simulation 3 uses the thermal expansion coefficient of the α phase while simulation 4 uses the thermal expansion coefficient of the β phase. Since generally the microstructure contains both phases (note that we consider that α and α' have the same value of linear thermal expansion), this allows to estimate the limits of the material's volume change.

Table 2 – Temperature independent material properties of Ti-6Al-4V.

Property	Solid	Powder	Liquid
ρ [kg/m^3]	4420	2652	4189
c_p [J/kg·K]	546	520	759
k [W/m·K]	7.0	0.145	28.4
E [GPa]	125	0.125	0.125
ν [-]	0.34	0.34	0.34
σ_Y [MPa]	1000	1.0	1.0

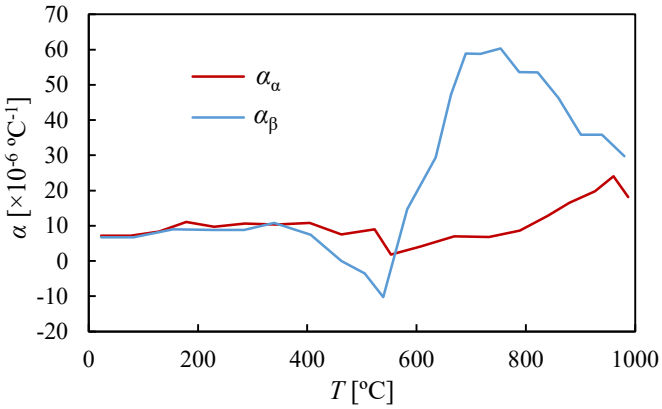

Fig. 2 – Temperature dependent thermal expansion coefficients for the α and β solid phases.

Results and Discussion

Fig. 3 presents the evolution of the volume fraction of each solid phase for simulations 1 and 2. The first heating cycle (1 s) is common to both simulations, corresponding to the heating of the powder phase past the melting point. During this heating and the cooling down to the melting point there are yet no solid phases. When the temperature drops below the melting point, the microstructure consists 100% of β phase. In simulation 1, since the cooling rate of the first cooling cycle is higher than 410 ºC/s, the microstructure at room temperature (t_2 = 2 s) consists almost entirely of α', containing also a residual volume fraction of β phase. In simulation 2, this critical cooling rate is not reached and, thus, there are only α and β phases at room temperature (64% of β and 36% of α, for t_2 = 16 s). The second heating cycle promotes martensite decomposition in simulation 1 (t_3 = 252 s), while no transformation occurs in simulation 2 (t_3 = 41 s), since the volume fraction of β is larger than the corresponding equilibrium volume fraction. In simulation 1, the second cooling cycle promotes

the β → α transformation, although only in a small percentage, due to insufficient time for diffusion. In simulation 2, the critical cooling rate is exceeded and the formation of α' is promoted in the second cooling cycle. The final microstructure of simulation 1 consists of 94.430% of α', 0.420% of β and 5.150% of α, while in simulation 2 there is 55.253% of α', 8.973% of β and 35.774% of α.

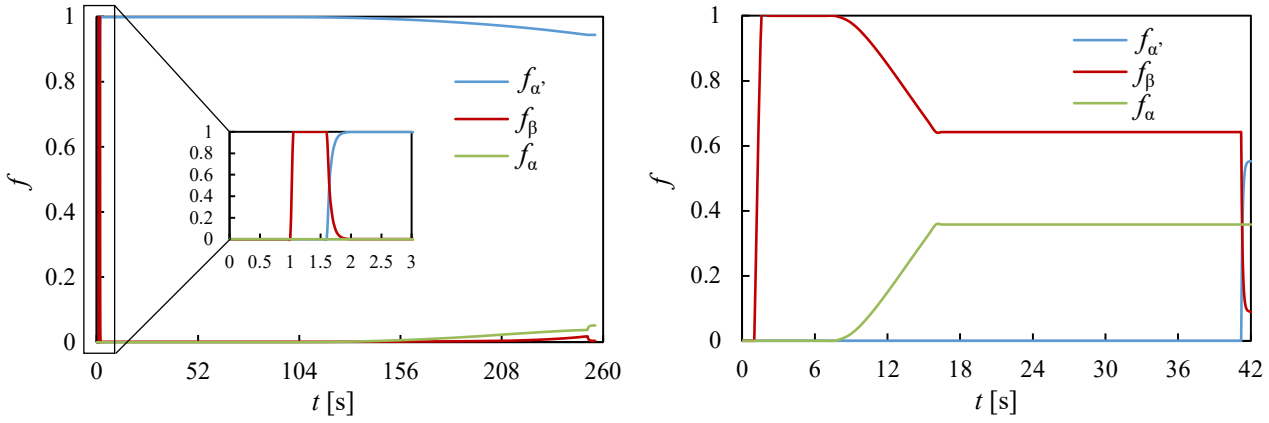

Fig. 3 – Predicted solid phase volume fractions: (a) Simulation 1; (b) Simulation 2.

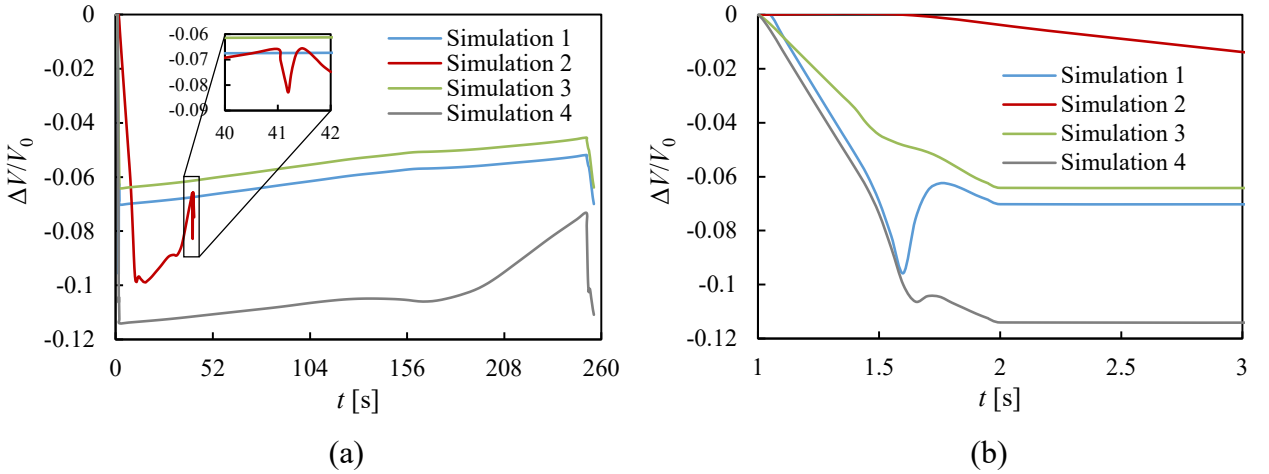

Fig. 4 – Predicted material volume change relative to the initial volume: (a) During the complete simulation; (b) Between t = 1 s and t = 3 s.

Fig. 4 shows the evolution of the cube's volume change relative to its initial volume for each simulation. The results of simulations 1 and 2 account for the thermal strains and the phase transformation strains, while the results of simulations 3 and 4 only consider thermal strains. During the first heating cycle and subsequent cooling down to the melting point, there is no thermal expansion in any simulation. In the remaining portion of the first cooling cycle, the thermal strain controls the volume evolution since the solid material contracts as it cools down. However, in simulation 1, the β → α' transformation is responsible for the material expansion from 1.65 s to 1.75 s. Once the transformation is almost completed, the material contracts until the end of the cooling cycle. In the second heating cycle, the solid material expands as the temperature increases (in all simulations). During the last cooling cycle, the material contracts as it cools down. Nonetheless, in simulation 2, between 41.25 s and 41.45 s, the β → α' transformation promotes material expansion. Simulation 4 shows some small oscillations in the volume change curve, which do not appear in simulation 3. This is due to the accentuated variation of the thermal expansion coefficient of the β phase (see Fig. 2).

For this particular thermal history, if the material was in solid state at the beginning, simulations 3 and 4 would have a relative volume change of zero after the thermal cycles (at t = 256 s). However, under the adopted conditions, at the end of the thermal cycles, simulations 3 and 4 have a residual

volume change of -6.4% and -11.1%, respectively. On the other hand, due to the effect of the solid-state phase transformations, simulations 1 and 2 show -7% and -7.5% of residual volume change, respectively. Since in simulations 1 and 2 the combined volume fractions of α' and α represent the majority of the microstructure, the predicted relative volume change is close to the one of simulation 3, which assumes 100% α phase. Although the example studied is very simple, it highlights that not predicting the microstructure evolution and its influence on the mechanical behavior can lead to incorrect estimation of the material's volume change. Changing the heating/cooling rates in simulations 1 and 2 resulted in completely different final microstructures, which showed a 0.5% difference on the material's volume change relative to its initial volume. Assuming a linear elastic behavior, this would correspond to a stress increment of approximately 200 MPa if the material was fully constrained. Under much more complex thermal histories, such as the ones associated to the SLM process, not predicting solid phase fields can potentially introduce significant errors in the estimation of the strain and stress fields.

Conclusions

In this work, a thermo-metallurgical-mechanical model is developed to predict the microstructure evolution of the Ti-6Al-4V alloy and its impact on the material's volume change (via thermal and phase transformation strains). Three solid phases are considered in the metallurgical model: α, β and α'. All material properties with exception of the thermal expansion coefficients are assumed temperature independent. The physical domain is meshed with a single finite element and two sequential heating/cooling cycles are applied, *via* heat fluxes, to obtain the desired temperature evolution (same temperature variation on all simulations). Four simulations are carried out, two considering phase-transformation induced strains and two only accounting for thermal strains.

The numerical results highlight the importance of microstructure prediction for an accurate estimation of the material's volume change. Without solid-state phase transformations, simulations considering the thermal expansion coefficient of the α and β phases have a residual volume change of -6.4% and -11.1%, respectively. In the simulations that account for solid transformations, changing the heating/cooling rates yielded completely different final microstructures. Consequently, the predicted volume change of the material relative to its initial volume showed a 0.5% difference, which would correspond to a stress increment of approximately 200 MPa if the linear elastic material was fully constrained.

Acknowledgements

The authors gratefully acknowledge the financial support of the projects POCI-01-0145-FEDER-031657 (PTDC/EME-EME/31657/2017) and UIDB/00285/2020 financed by the Operational Program for Competitiveness and Internationalization, in its FEDER/FNR component, and the Portuguese Foundation of Science and Technology (FCT), in its State Budget component (OE). The first author is also grateful to the FCT for the PhD grant with reference 2020.07178.BD.

References

[1] S. Liu and Y. C. Shin, "Additive manufacturing of Ti6Al4V alloy: A review," *Mater. Des.*, vol. 164, p. 107552, 2019.

[2] L. Thijs, F. Verhaeghe, T. Craeghs, J. Van Humbeeck, and J. P. Kruth, "A study of the microstructural evolution during selective laser melting of Ti-6Al-4V," *Acta Mater.*, vol. 58, no. 9, pp. 3303–3312, 2010.

[3] N. Kazantseva, P. Krakhmalev, M. Thuvander, I. Yadroitsev, N. Vinogradova, and I. Ezhov, "Martensitic transformations in Ti-6Al-4V (ELI) alloy manufactured by 3D Printing," *Mater. Charact.*, vol. 146, no. February 2020, pp. 101–112, 2018.

[4] J. Yang, H. Yu, J. Yin, M. Gao, Z. Wang, and X. Zeng, "Formation and control of martensite in Ti-6Al-4V alloy produced by selective laser melting," *Mater. Des.*, vol. 108, pp. 308–318, 2016.

[5] S. Cao, Y. Zou, C. Voon Samuel Lim, and X. Wu, "Review of laser powder bed fusion (LPBF) fabricated Ti-6Al-4V: process, post-process treatment, microstructure, and property," *Light Adv. Manuf.*, vol. 2, no. 2, pp. 1–20, 2021.

[6] M. Simonelli, Y. Y. Tse, and C. Tuck, "The formation of α + β microstructure in as-fabricated selective laser melting of Ti-6Al-4V," *J. Mater. Res.*, vol. 29, no. 17, pp. 2028–2035, 2014.

[7] M. M. Francois *et al.*, "Modeling of additive manufacturing processes for metals: Challenges and opportunities," *Curr. Opin. Solid State Mater. Sci.*, vol. 21, no. 4, pp. 198–206, 2017.

[8] P. Tan, F. Shen, B. Li, and K. Zhou, "A thermo-metallurgical-mechanical model for selective laser melting of Ti6Al4V," *Mater. Des.*, vol. 168, p. 107642, 2019.

[9] Y. Fan, P. Cheng, Y. L. Yao, Z. Yang, and K. Egland, "Effect of phase transformations on laser forming of Ti-6Al-4V alloy," *J. Appl. Phys.*, vol. 98, no. 1, pp. 1–10, 2005.

[10] D. P. Koistinen and R. E. Marburger, "A general equation prescribing the extent of the austenite-martensite transformation in pure iron-carbon alloys and plain carbon steels," *Acta Metall.*, vol. 7, no. 1, pp. 59–60, 1959.

[11] M. Avrami, "Kinetics of Phase Change. I General Theory," *J. Chem. Phys.*, vol. 7, no. 12, pp. 1103–1112, Dec. 1939.

[12] M. J. Donachie, *Titanium: A Technical Guide*, 2nd Ed. ASM International, 2000.

[13] T. Ahmed and H. J. Rack, "Phase transformations during cooling in α + β titanium alloys," *Mater. Sci. Eng. A*, vol. 243, no. 1–2, pp. 206–211, 1998.

[14] C. Leyens and M. Peters, *Titanium and Titanium Alloys*. Wiley-VCH, 2003.

[15] J. Xie and J. A. Hurtado, "Phase Transformations in Metals during Additive Manufacturing Processes," in *NAFEMS World Congress*, 2017.

[16] A. Crespo, A. Deus, and R. Vilar, "Modeling of phase transformations and internal stresses in laser powder deposition," *XVII Int. Symp. Gas Flow, Chem. Lasers, High-Power Lasers*, vol. 7131, p. 713120, 2008.

[17] Q. Zhang, J. Xie, Z. Gao, T. London, D. Griffiths, and V. Oancea, "A metallurgical phase transformation framework applied to SLM additive manufacturing processes," *Mater. Des.*, vol. 166, 2019.

[18] F. X. Gil Mur, D. Rodríguez, and J. A. Planell, "Influence of tempering temperature and time on the α′-Ti-6Al-4V martensite," *J. Alloys Compd.*, vol. 234, no. 2, pp. 287–289, 1996.

[19] L. Seraphin and R. Castro, "Contribution to metallographic and structural study of titanium alloy TA6V," *Mem. Sci. la Rev. Metall.*, no. 63, pp. 1025–1058, 1966.

[20] G. Marion, G. Cailletaud, C. Colin, and M. Mazière, "A finite element model for the simulation of direct metal deposition," *Int. Congr. Appl. Lasers Electro-Optics*, vol. 2014, no. 1, pp. 834–841, Oct. 2014.

[21] S. Malinov, P. Markovsky, W. Sha, and Z. Guo, "Resistivity study and computer modelling of the isothermal transformation kinetics of Ti-6Al-4V and Ti-6Al-2Sn-4Zr-2Mo-0.08Si alloys," *J. Alloys Compd.*, vol. 314, no. 1–2, pp. 181–192, 2001.

[22] J. W. Elmer *et al.*, "In-Situ Observations of Phase Transformations in the Fusion Zone of Ti-6Al-4V Alloy Transient Welds Using Synchrotron Radiation," *Tms*, pp. 1–30, 2005.

[23] J. W. Elmer, T. A. Palmer, S. S. Babu, and E. D. Specht, “In situ observations of lattice expansion and transformation rates of α and β phases in Ti-6Al-4V,” *Mater. Sci. Eng. A*, vol. 391, no. 1–2, pp. 104–113, 2005.

[24] L. F. Menezes and C. Teodosiu, “Three-dimensional numerical simulation of the deep-drawing process using solid finite elements,” *J. Mater. Process. Technol.*, vol. 97, no. 1–3, pp. 100–106, Jan. 2000.

[25] J. M. P. Martins, J. L. Alves, D. M. Neto, M. C. Oliveira, and L. F. Menezes, “Numerical analysis of different heating systems for warm sheet metal forming,” *Int. J. Adv. Manuf. Technol.*, vol. 83, no. 5–8, pp. 897–909, Mar. 2016.

[26] T. J. R. Hughes, “Generalization of selective integration procedures to anisotropic and nonlinear media,” *Int. J. Numer. Methods Eng.*, vol. 15, no. 9, pp. 1413–1418, Sep. 1980.

[27] K. C. Mills, *Recommended values of thermophysical properties for selected commercial alloys*. Woodhead Publishing Limited, 2002.

[28] J. L. P. Rangaswamy, H. Choo, M. Prime, M. Bourke, “High Temperature Stress Assessment in SCS-6/Ti-6Al-4V Composite using Neutron Diffraction and Finite Element Modeling,” in *THERMEC 2000 International Conference*, 2000.

[29] L. Parry, I. A. Ashcroft, and R. D. Wildman, “Understanding the effect of laser scan strategy on residual stress in selective laser melting through thermo-mechanical simulation,” *Addit. Manuf.*, vol. 12, pp. 1–15, Oct. 2016.

[30] Z. Zhang *et al.*, “3-Dimensional heat transfer modeling for laser powder-bed fusion additive manufacturing with volumetric heat sources based on varied thermal conductivity and absorptivity,” *Opt. Laser Technol.*, vol. 109, pp. 297–312, Jan. 2019.